PERGAMON

International Journal of Solids and Structures 40 (2003) 1299–1310

INTERNATIONAL JOURNAL OF SOLIDS and STRUCTURES

www.elsevier.com/locate/ijsolstr

Interfacial friction in the debonded structural cell of particulate rubber composites

A.S. Koltsov *, V.A. Sursjakov, V.V. Moshev

Ural Department of Russian Academy of Sciences, Institute of Continuous Media Mechanics, 1 Korolev Street, Moscow 614013, Russia

Received 27 March 2001; received in revised form 19 September 2002

Abstract

The role of the interface friction in formation of mechanical behavior of structural cells is examined. A method for calculation of the stress–strain state induced by the interface friction within the debonded structural cells is presented. Features of the structural stresses and strains are presented and the localities of the microdamage onsets are established. Effective properties of cells are determined and their dependence on the interface friction is demonstrated.

Keywords: Structural modeling; Particular rubber composites; Contact problem

1. Introduction

The problem of searching representative volume elements in materials degrading under deformation has become an object of numerous publications in the last years. It is generally recognized that the microstructure damage events based on sound physical postulates help in explaining complicated macroscopic mechanical behavior of various materials. This situation is clearly represented in recent reviews of Murakami and Liu (1996) and Broberg (1997). The specificity of particular materials (polycrystalline metals and alloys, concrete, rock, polymeric composites) gives rise to a wide variety of approaches used. Most of papers are focused on such materials as polycrystalline metals and alloys, concrete, rock, and rigid composites.

Papers concerning polymeric particulate composites are scanty. Structural cells are often considered as some phenomenological objects (black boxes) whose behavior is derived mainly or partly from macroscopic behavior of appropriate materials (Anderson Vratsanos and Farris, 1993a,b; Liu et al., 1998). Hence, the development of a cell as material unit, that contain sufficient information for predicting macroscopic behavior of a material and, at the same time, is based on physical concepts without enlisting macroscopic notions, may be regarded as a vital problem in today's material science.

* Corresponding author. Fax: +7-3422-336957.
E-mail address: kasi@icmm.ru (A.S. Koltsov).

0020-7683/02/$ - see front matter
PII: S0020-7683(02)00581-4

Nomenclature

L	height of the cell (mm)
D	diameter of the cell (mm)
R	radius of spherical inclusion (mm)
φ	volume fraction of the spherical inclusion in the cell
p	external hydrostatic pressure (MPa)
U	one half of displacement value between the ends of the cell (mm)
F	axial force value applied to the ends of the cell (N)
W	strain energy function (MPa)
μ	shear modulus (material constant) (MPa)
B	bulk modulus (material constant) (MPa)
α	compressibility parameter of the matrix (MPa^{-1})
f	friction force per area unit (MPa)
T	constant in the adopted friction law (MPa)
β	constant in the adopted friction law (MPa^{-1})
V_0	volume of the unstrained cell (mm^3)
S_p^0	the unstrained cell surface (mm^2)
$\boldsymbol{u}$	displacement vector (mm)
u_τ	tangential component of $\boldsymbol{u}$
Δu_τ	increment of u_τ on step of cell's extension
$\boldsymbol{r}$	radius-vector of points in the initial state (mm)
$\boldsymbol{G}$	Cauchy–Green deformation measure tensor
I_1, I_3	invariants of **G**
$\boldsymbol{k}$	vector of the surface forces reduced to the initial state (MPa)
$\boldsymbol{Q}$	energy stress tensor (MPa)
$\boldsymbol{P}$	second Piola–Kirchoff stress tensor (MPa)
σ	true stress tensor (MPa)
σ_n, σ_τ	interfacial normal and tangential contact stresses (MPa)
$H(h, \boldsymbol{u})$	functional used in the model
h	parameter of the state equation (MPa)
λ_1	is the maximum principal stretch
ε_1	the maximum principal strain
s_0	mean stress (MPa)

Our efforts in the last few years have been focused exactly on this point, damageable particulate polymeric composites being the object of research (Kozhevnikova et al., 1993; Moshev and Kozhevnikova, 1996a,b, 1997). In this approach, cells are considered as systems with a rather complicated internal substructure whose macroscopic behavior is deduced from the solution of appropriate boundary-value problems. Such way of looking allows obtaining a large body of important information concerning structural damage, explains some features of macroscopic behavior of particulate composites and creates a more sound bridge in the field of the structure-properties gap. The satisfactory adequacy of the approach has been evidenced by good agreement between theoretical and experimental concentration curves for relative macroscopic modulus.

This gave impetus to further refining the model under consideration. In earlier papers, it was assumed that no interface friction existed between debonded matrix and filler particles, whereas it is well known that

this factor sometimes can play considerable role, say under superimposed pressure. With this in mind, a closer attention has been drawn to elucidation how the interface friction influences the mechanical behavior of structural cells. This point is the goal of the present paper.

2. Theoretical background

2.1. Model cell geometry and boundary conditions

The construction of the representative structural cell has been substantiated in Moshev and Kozhevnikova (2000). Its general scheme is shown in Fig. 1(a). The cell represents an elastomeric cylinder (matrix), containing a solid spherical inclusion (filler particle) at the center. The height, L, of the cylinder equals its diameter, D. The cell is loaded by tension along the axis of the cylinder. It is supposed that initially the cell is well compacted with other cells of the same size (Fig. 1(b)) and continues to retain this state under tension. Meeting this requirement makes ends of the cell remain plane and its lateral surface keep cylindrical shape during extension. The matrix and the inclusion are assumed to be initially debonded.

2.2. Testing conditions

The cell is tested in simple tension or compression under a constant superimposed (external) pressure. The current mechanical state of the cell is, thus, determined by two testing parameters: cell's extension $2U$ and external pressure p.

2.3. Mechanical properties of constituent elements

The matrix phase is represented by a slightly compressible elastomer characterized by the elastic potential, W, having the form (Kozhevnikova et al., 1993)

$$W = \frac{\mu}{2}(I_1 - (I_3 - 1) - 3) + \frac{1}{2\alpha}(I_3 - 1)^2, \tag{1}$$

where

$$\alpha = \frac{12}{3B + 4\mu}, \tag{2}$$

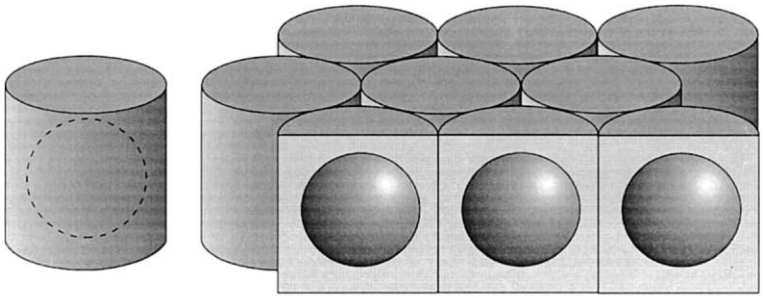

Fig. 1. General scheme of the structural cell (a) and its packing condition (b).

where μ is a material constant, whose value is taken equal to 1 MPa, which corresponds to the shear modulus at small deformations; B is a second material constant that may be regarded as a bulk modulus at small deformations, whose value is taken to be 50 MPa, which corresponds to Poisson's ratios about 0.4966; I_1 and I_3 are the first and the third invariants of the Cauchy–Green deformation measure tensor.

Corresponding constitutive equation derived from (1) is represented as

$$\frac{1}{2}\sqrt{I_3}\boldsymbol{Q} = \frac{\partial W}{\partial \boldsymbol{G}}, \tag{3}$$

with

$$\boldsymbol{Q} = \boldsymbol{P}\frac{1}{\sqrt{I_3}}, \tag{4}$$

where $\boldsymbol{Q}$ is the tensor of energy, $\boldsymbol{P}$ is the second Piola–Kirchoff stress tensor, $\boldsymbol{G}$ is the Cauchy–Green deformation measure tensor.

The solid sphere is taken to be perfectly rigid. Hence all the energy of deformation of the cell is stored within the matrix volume.

2.4. Interfacial friction law

Experiments described in Moshev and Kovrov (1998) made possible derivation of an empirical formula relating specific friction force with the applied pressure and rate of sliding. A simplified form of this relation, taking into account only pressure sensitivity of the friction force, has been used in forthcoming calculations

$$f = T(1 - \exp(\beta\sigma_n)), \tag{5}$$

where f is friction force per area unit, T and β are empirical constants. In this paper, the value of T (in MPa) was chosen in conformity with the matrix adopted rigidity μ through keeping the same ratio as was established in the above paper. Parameter β, reflecting the nonlinear response of the friction force to pressure, has been taken equal to 8.0 as it was determined in the experiments mentioned.

2.5. Statement of the problem

The problem under consideration is axisymmetric. Hence a quarter of the cell is enough for calculations in problem solving. An appropriate scheme is depicted in Fig. 2. Mathematical treatment is carried out in the cylindrical coordinate system.

The boundary conditions in this scheme are imposed as follows:

AB: $u_r = 0$, $\sigma_{rz} = 0$,
BC: $u_z = U$, $\sigma_{rz} = 0$, where U is the input parameter in the problem to be examined,
CD: $u_r = \text{const}$, $\frac{1}{S_{\text{CD}}}\int_{\text{CD}} \sigma_{rr}\,\mathrm{d}S_{\text{CD}} = -p$, $\sigma_{rz} = 0$, where u_r is the output parameter searched,
DE: $u_z = 0$, $\sigma_{rz} = 0$,

where u_z, u_r and σ_{rz}, σ_{rr} is components of displacement vector ($\boldsymbol{u}$) and true stress tensor (σ).

The interface EA may be either in the closed (EH) or in the open (HA) states. Hence, conditions along EA line are expressed as follows:

$$(|\boldsymbol{r} + \boldsymbol{u}| - R) \geqslant 0, \tag{6.1}$$

$$\sigma_n \leqslant 0, \tag{6.2}$$

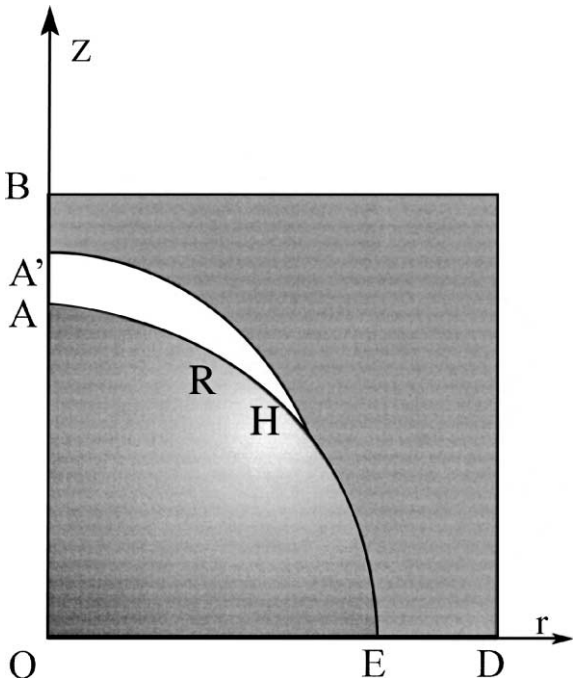

Fig. 2. Scheme of the quarter of the cell depicting boundary conditions.

$$(|\boldsymbol{r}+\boldsymbol{u}|-R)\sigma_n = 0, \tag{6.3}$$

$$f = T(1-\exp(\beta\sigma_n)), \tag{7.1}$$

$$\Delta u_\tau(|\sigma_\tau| - f) = 0, \tag{7.2}$$

$$|\sigma_\tau| \leqslant f, \tag{7.3}$$

$$\text{if } |\sigma_\tau| = f, \quad \text{then } \frac{\sigma_\tau}{|\sigma_\tau|} = -\frac{\Delta u_\tau}{|\Delta u_\tau|}, \tag{7.4}$$

where $\boldsymbol{r}$—radius-vector of points in the initial state, R—radius of spherical inclusion, u_τ—tangential component of $\boldsymbol{u}$, Δu_τ—increment of U_τ on step of cell's extension, σ_n, σ_τ—interfacial normal and tangential contact stresses.

2.6. Calculation procedure

The value of U was used as an input parameter in the calculation procedure with the consequent establishment of u_r meeting other imposed boundary condition p.

For problem solving, a functional $(H(h,\boldsymbol{u}))$ of a special form suggested by Kozhevnikova et al. (1993) has been used

$$H(h,\boldsymbol{u}) = \int_{V_0}\left\{h(I_3-1) + W + \frac{\alpha}{2}h^2\right\}\mathrm{d}V_0 - \int_{S_p^0}\boldsymbol{k}\cdot\boldsymbol{u}\,\mathrm{d}S_p^0, \tag{8}$$

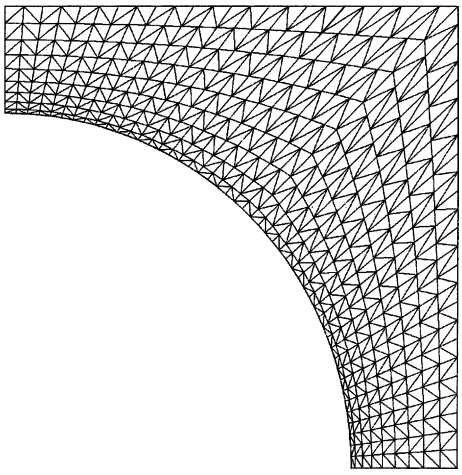

Fig. 3. Typical sketch of the adopted finite element grid for $\varphi = 30\%$ solid volume fraction.

where h is regarded as a mean stress, and

$$h = \frac{1}{\alpha}(I_3 - 1), \tag{9}$$

$\boldsymbol{k}$—vector of the surface forces reduced to the initial state, V_0—volume of the unstrained cell, S_p^0—the unstrained cell surface.

The finite element method was used for calculations. A typical sketch of the adopted finite element grid is shown in Fig. 3 for a solid volume fraction (φ) of 30%. Considering the geometry of the cell, a condensation of elements near the inclusion was performed.

A program was developed for the incremental load procedure, using triangular cylindrical finite elements with a linear approximation to the displacement field, and step function h.

Contact zones were found by means of the effective iteration algorithm (Uzawa's Arrow et al., 1958) treating interface contact conditions and with sweeping contact forces.

3. Analysis and discussion

3.1. Microstrains and microstresses in the matrix and at the interface

The following geometrical, material, and operation parameters were used in the analysis: the height of the cell $L = 2$ mm, the diameter of the cell $D = 2$ mm, matrix elasticity parameters $\mu = 1$ MPa and $B = 50$ MPa; sliding friction parameters $T = 0 \sim 1.0$ MPa, $\beta = 8.0$ MPa^{-1}; filler volume fraction $\varphi = 20\%$, 30%, 40%; surrounding pressure $p = 0 \sim 1.0$ MPa.

The influence of two test parameters, i.e., the cell's extension, U, and the external pressure, p, is examined.

Remembering that the spherical inclusion as a constituent of the structural cell is taken to be perfectly rigid and nondestructive, the analysis of the internal state of the cell will cover only the examination of the stress–strain state of the matrix, interfacial stresses and strains and the volume changes of the cell caused by the proper matrix compressibility and induced by vacuole appearance and evolution.

Two representative quantities of the stress–strain state of the rubbery matrix are chosen for further analysis (Moshev and Kozhevnikova, 1996a,b): the maximum principal strain, ε_1, as an invariant characterizing the *intensity of deformation* and the mean stress, s_0, as a measure of *hydrostatic intensity of stress state*. In this paper, the value of ε_1 is presented as $\varepsilon_1 = \lambda_1 - 1$, where λ_1 is the maximum principal stretch. The value of s_0 is mean of three principal true stresses.

Most of the quantitative data to be presented in the subsequent analysis as illustrations have been obtained from calculations for a cell containing solid phase of $\varphi = 30\%$ by volume extended by 50%.

Figures present ε_1 and s_0 distributions for imposed conditions as shadow patterns: the higher the level of the strain or stress the lighter the shadow. Such patterns are to be regarded primarily as qualitative estimations for getting general orientation with most important numerical data indicated in critical localities.

Each figure consists of two patterns. The first one (a) represents frictionless situation, the second (b) reflects the same case except that the friction of $T = 1.0$ MPa is accounted for.

Fig. 4 compares strain ε_1 of frictionless (a) and frictional (b) case at zero external pressure p. It is seen that accounting for friction influence does not change markedly the general strain distribution. A weakly strained dome like region above detached part of the matrix passes into a more strained zone around the equator of the inclusion, where strain maxima are disposed. In Fig. 4(b) maximum strain of $\varepsilon_1 = 1.63$ is considerably higher than that in Fig. 4(a) equal to $\varepsilon_1 = 1.10$. As well, the locations of these maxima are different. In the absence of friction, maximum strain is situated along the equatorial line, while, in the presence of friction, maximum strain shifts to the tip of the crack.

Fig. 5 compares frictionless (a) and frictional (b) strain states at the external pressure of 1.0 MPa. It is seen that, though the general strain patterns resemble each other, distinct changes take place in the equatorial zone, where the maximum strains, both in (a) and (b), are displaced to the equatorial boundary of the cylinder with friction-case of 1.69 being slightly greater than no-friction one of 1.66.

Figs. 6 and 7 demonstrate the effect of friction f changes s_0 on the distribution of the mean stress s_0. In all instances maximum values of s_0 are located at the tips of the cracks. At zero external pressure (Fig. 6), maximum s_0 of the friction-case is $s_0 = 3.28$ MPa that is markedly higher than the no-friction case of $s_0 = 1.29$ MPa. The like interdependence is observed at the external pressure of $p = 1.0$ MPa (Fig. 7), where the maximum s_0 of the friction-case is equal to 2.44 MPa that again is higher than $s_0 = 0.70$ MPa of the no-friction case with the both values considerably lower than the same quantities of Fig. 6.

The general overview on the joint influence of friction force f and external pressure p on the maximum values of ε_1 at filler volumes $\varphi = 20\%$, 30% and 40% is depicted in Fig. 8. At lower φ of 20% solid volume

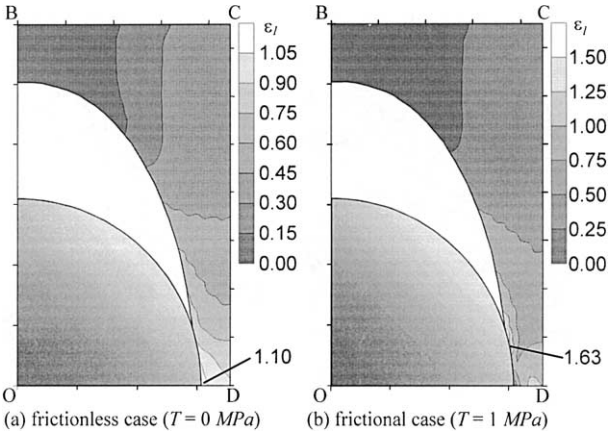

Fig. 4. Comparison of strain ε_1 between frictionless case (a) and frictional case (b) at zero external pressure.

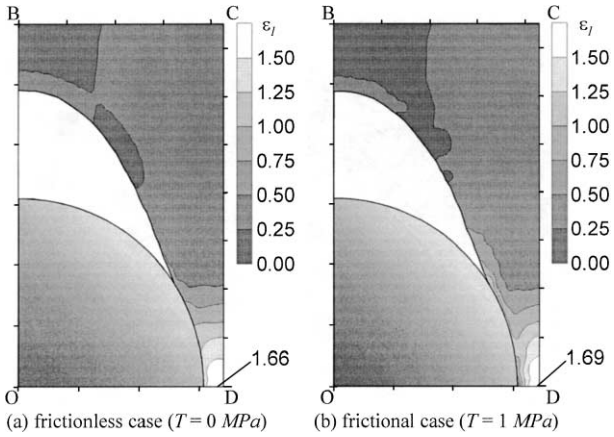

Fig. 5. Comparison of strain ε_1 between frictionless case (a) and frictional case (b) at the external pressure $p = 1.0$ MPa.

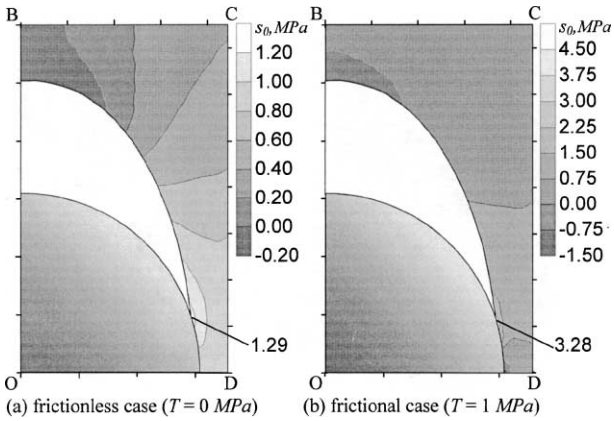

Fig. 6. Comparison of stress s_0 between frictionless case (a) and frictional case (b) at zero external pressure.

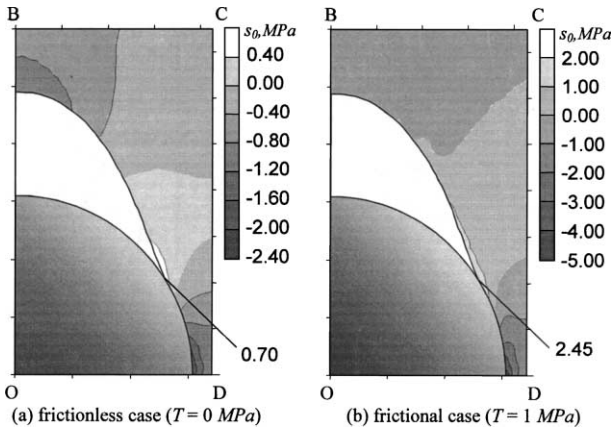

Fig. 7. Comparison of strain s_0 between frictionless case (a) and frictional case (b) at the external pressure $p = 1.0$ MPa.

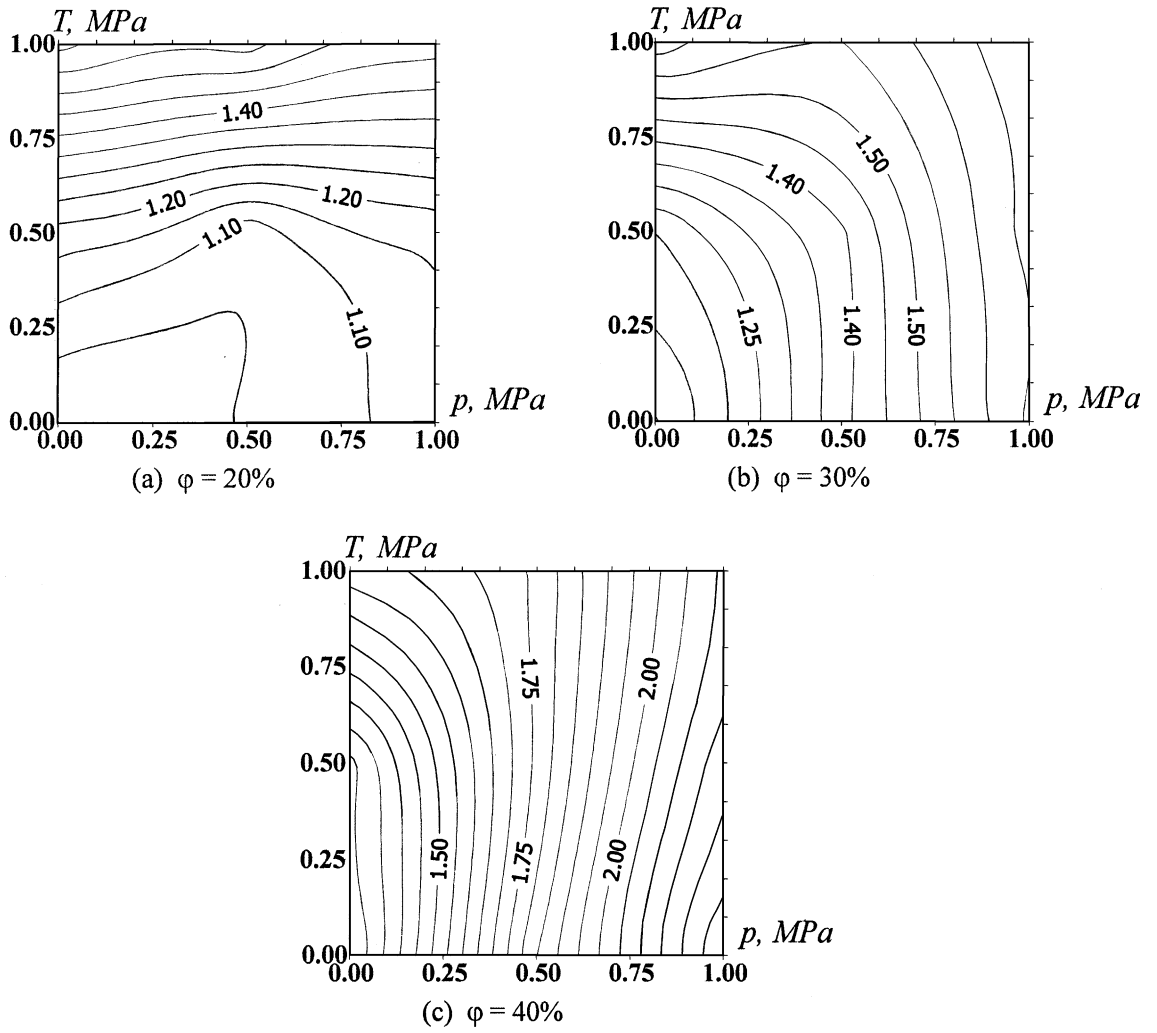

Fig. 8. Joint influence of friction T and external pressure p on the maximum values of ε_1 at filler volumes $\varphi = 20\%$, 30% and 40%.

fraction, f is the main controlling parameter, whereas at higher solid volume factions $\varphi = 30\%$ and 40% it is the external pressure that primarily determines maximum ε_1 magnitudes.

Calculations have shown that distributions of s_0 for various solid volume fractions are by and large similar. Typically they look for $\varphi = 30\%$ solid volume fraction as in Fig. 9. It is seen that both friction and external pressures rise the largest value of s_0 with friction force being the main controlling factor.

3.2. Effective characteristics of the structural cell

The former analysis has been focused on the internal stress and strain states in structural cells under tension. An application of *structural notions and relations*, used in solutions of boundary-value problems, to corresponding *macroscopic characteristics* of cells is the next step to continuum formulations.

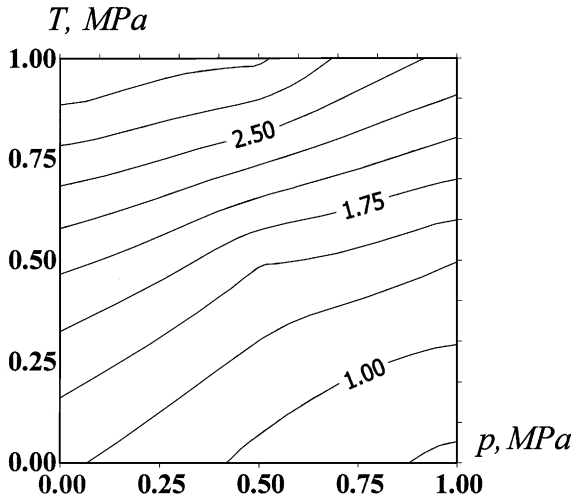

Fig. 9. Joint influence of friction T and external pressure p on the maximum values of s_0 at filler volumes $\varphi = 30\%$.

For this, a substitution of the microstresses, σ, and microstrains, ε, that have been used, say, for inside-cell analysis, for macroscopic axial force F and axial displacement U of a larger scale level, i.e., that of the cell characteristic size, is needed.

So far only tension tests have been investigated. However, after having passed to continuum generalization, it becomes of interest to examine not only the extension behavior but also the compressive one with a view to evaluate hysteresis loss caused by the interface friction phenomenon. Fig. 10 depicts four curves of the tension–compression type calculated for two external pressures ($p = 0$ and 1 MPa) and two frictional levels ($T = 0$ and 1 MPa) for $\varphi = 30\%$ solid volume fraction. It follows from this figure that hysteresis loss is strongly dependent on the external pressure magnitude p. The reason is that they are tightly coupled with

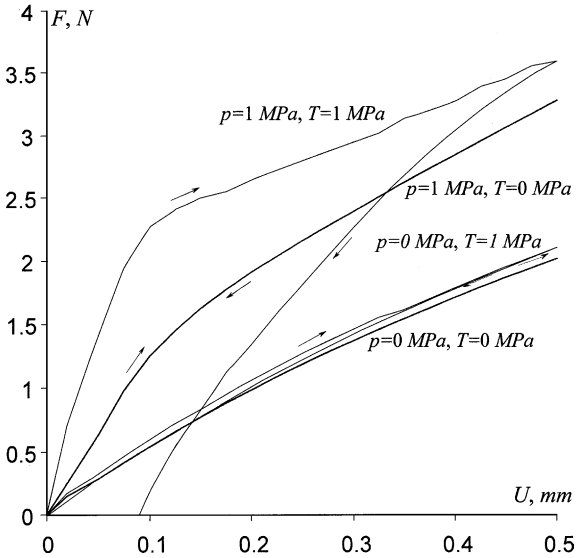

Fig. 10. Tension–compression curves for $p = 0$ and $p = 1.0$ MPa at zero friction ($T = 0$ MPa) and friction $T = 1.0$ MPa.

the value of the interface contact area that increases considerably with the external pressure. The hysteresis loss is negligible at zero external pressure, characterized by a small equatorial contact area that agree well with the experiments (Moshev, 1991).

Hence increasing filler volume fraction must increase the effect induced by the interfacial friction due to the rising the contact interface area at the same external pressure. This is validated by Fig. 11, where two hysteresis curves for $\varphi = 20\%$ and 30% solid volume fractions are compared.

It may be suggested that the volume change, as a function of elongation, should depend only slightly on the interface friction when comparing friction and no-friction cases under other similar conditions. The calculations confirm this assumption. Fig. 12 presents volume expansion ratio (V/V_0) as a function of the cell elongation, where V is the current volume of cell, V_0 is the initial volume of cell (before applying external pressure).

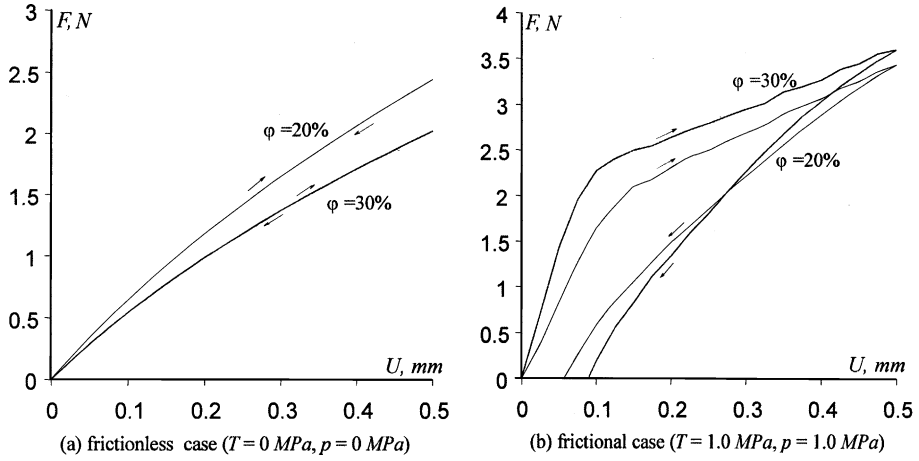

Fig. 11. Influence of filler volume fraction ($\varphi = 20\%$ and 30%) on the tension–compression curves: (a) frictionless case ($T = 0$ MPa, $p = 0$ MPa), (b) frictional case ($T = 1.0$ MPa, $p = 1.0$ MPa).

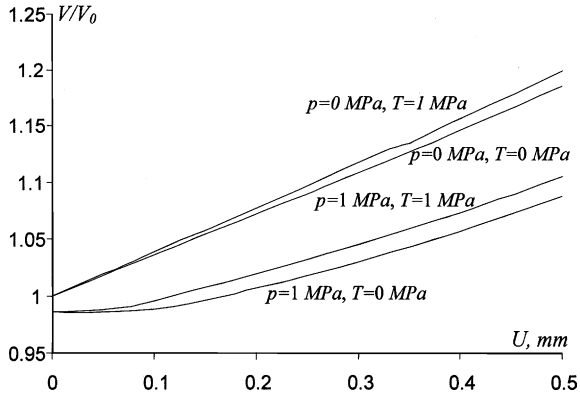

Fig. 12. Volume expansion ratio (V/V_0) as a function of elongation for $p = 0$ and $p = 1.0$ MPa at zero friction ($T = 0$ MPa) and friction equal to 1 ($T = 1.0$ MPa).

4. Discussion

The data obtained in this work allow one to evaluate the influence of the interface friction on the mechanical behavior of the model structural cell. Not to complicate the analysis of this phenomenon by accounting for the commonly observed interface separation, the cell was adopted to be debonded from the outset.

The analysis of the microstructural stresses and strains during the extension of the cell under combined action of the friction force f and the external pressure p shows that both f and p considerably increase strains as compared with the frictionless case.

The magnitude of energy dissipation, as, for instance, shown in Fig. 10, is strongly sensitive to the external pressure due to rising the frictional area. It is obvious that lowering the friction force to zero decreases the frictional losses to zero as well at any imposed external pressure.

5. Conclusions

- A method for calculation of microstresses and microstrains induced by the interface friction within the debonded structural cells is offered.
- Features of the structural stresses and strains are examined and the localities of the microdamage onsets are established.
- An examination of the interface dissipative loss as a function of the magnitudes of frictional force and the external pressure is carried out.
- The dependence of effective properties of the cells on the interface friction is demonstrated.

References

Anderson Vratsanos, L., Farris, R.J., 1993a. A predictive model for the mechanical behavior of particulate composites. Part I: Model derivation. Polym. Eng. Sci. 33, 1458–1465.

Anderson Vratsanos, L., Farris, R.J., 1993b. A predictive model for the mechanical behavior of particulate composites. Part II: Comparison of model predictions to literature data. Polym. Eng. Sci. 33, 1466–1474.

Arrow, K.J., Hurwicz, L., Uzawa, H., 1958. Studies in Linear and Nonlinear Programming. Stanford University Press.

Broberg, K.B., 1997. The cell model of materials. Comput. Mech. 19, 447–452.

Kozhevnikova, L.L., Moshev, V.V., Rogovoy, A.A., 1993. A continuum model for finite void growth around spherical inclusion. Int. J. Solid Struct. 30, 237–248.

Liu, Y., Kageyama, Y., Murakami, S., 1998. Creep fracture modeling by use of continuum damage variable based on Voronoi simulation of grain boundary cavity. Int. J. Mech. Sci. 40, 147–158.

Moshev, V.V., 1991. Interfacial friction in filled polymers initiated by adhesive debonding. J. Adhes. 35, 181–186.

Moshev, V.V., Kovrov, V.N., 1998. Interfacial friction in filled polymers initiated by adhesive debonding. II.I Physical modeling. J. Adhes. 65, 91–103.

Moshev, V.V., Kozhevnikova, L.L., 2000. Predictive potentialities of a cylindrical structural cell for particulate elastomeric composites. Int. J. Solids Struct. 37, 1079–1097.

Moshev, V.V., Kozhevnikova, L.L., 1996a. Pressure reinforcement of particulate polymeric composites originated by adhesive debonding. J. Adhes. 55, 197–207.

Moshev, V.V., Kozhevnikova, L.L., 1996b. Unit cell evolution in structurally damageable particulate-filled elastomeric composites under simple tension. J. Adhes. 55, 209–219.

Moshev, V.V., Kozhevnikova, L.L., 1997. Highly predictive structural cell for particulate polymeric composites. J. Adhes. 62, 169–186.

Murakami, S., Liu, Y., 1996. Local approach of fracture based on continuum damage mechanics and the related problems. Mater. Sci. Res. Int. 2, 131–142.